nature nanotechnology

SUPPLEMENTARY INFORMATION

DOI: 10.1038/NNANO.2011.66

In situ Formation of Highly Conducting, Covalent Au-C Contacts for Single Molecule Junctions

Z-L Cheng[1], R. Skouta[1], H. Vazquez[2], J. R. Widawsky[3], S. Schneebeli[1], W. Chen[1], M.S.Hybertsen[4], R.Breslow[1,2], L.Venkataraman[2,3].

[1]*Department of Chemistry, Columbia University*
[2]*Center for Electron Transport in Molecular Nanostructures, Columbia University*
[3]*Department of Applied Physics and Applied Mathematics, Columbia University*
[4]*Center for Functional Nanomaterials, Brookhaven National Laboratory*

Email: mhyberts@bnl.gov; rb33@columbia.edu; lv2117@columbia.edu

Contents:

Synthesis Information:

Chemicals: Solvents, inorganic salts, and organic reagents were purchased from commercial sources and used without further purification unless otherwise mentioned.

Chromatography: Merck pre-coated 0.25 mm silica plates containing a 254 nm fluorescence indicator were used for analytical thin-layer chromatography. Flash chromatography was performed on 230-400 mesh silica (SiliaFlash® P60) from Silicycle.

Preparative HPLC was run on a Waters 600 liquid chromatography system equipped with a WatersTM 600 pumping system and a Waters 2489 UV-Vis detector. Samples were collected manually. A Waters XBridgeTM C18 reverse phase preparative column (particle size 5 μm, 19x150 mm) was used as stationary phase.

Spectroscopy: NMR spectra were obtained on a Bruker DPX 300 or 400 MHz spectrometer. Spectra were analyzed with the MestreNova Software (Version 6.1).

CI-MS spectra were taken on a Nermag R-10-10 instrument.

Synthesis of $SnMe_3$ Alkanes: The $SnMe_3$-terminated alkanes used in this study were prepared by coupling the corresponding di-Grignard reagents with $SnMe_3Cl$ following known procedures in the literature[1,2] as illustrated in the scheme below.

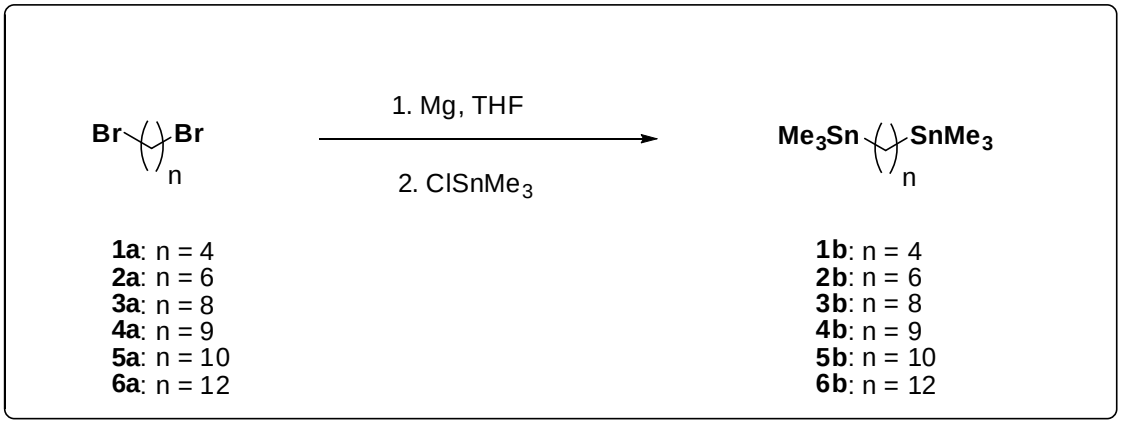

1a: n = 4
2a: n = 6
3a: n = 8
4a: n = 9
5a: n = 10
6a: n = 12

1b: n = 4
2b: n = 6
3b: n = 8
4b: n = 9
5b: n = 10
6b: n = 12

General Protocol:

To a suspension of 10 equiv of Mg and a small crystal of I_2 in dry THF (60 mL) was added a solution of various dibromoalkanes (1 equiv) in THF (20 mL) over 1.5-2 h at 15-20^{o}C. After 8 h stirring at room temperature, the bis(bromomagnesio)alkane solution was

separated from excess Mg by cannula transfer. A solution of 2 equiv of trimethylstannyl chloride in THF (1.0 M) was added over a period of 1h to the Grignard solution at 0°C. The mixture was allowed to warm to 25°C, and then heated for 2 h at 50°C. The mixture was cooled to 0°C and hydrolyzed with a saturated aqueous solution of ammonium chloride. The organic phase was separated and the aqueous phase was extracted three times with 20 mL of diethylether. After drying with anhydrous magnesium sulfate the solvents were removed under vaccum. The crude oil was purified by silica gel.

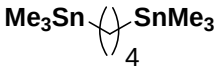

1,4-Bis(trimethylstannyl)butane (1b). Following the above general procedure with 1,4 dibromobutane **1a** (1 mL, 8.37 mmol), Mg (2.03 g, 83.7 mmol) and trimethylstannyl chloride 1.0 M in THF (16.7 mL, 16.7 mmol), the crude reaction mixture was purified by column chromatography (hexane) to provide the colorless oil **1b** (800 mg, 2.07 mmol, 24%). ^{1}H NMR ($CDCl_3$, 400MHz, ppm) δ 1.60-1.40 (m, 4H), 0.95-0.65 (m, 4H), 0.04 (t, J = 24 Hz, 18H); ^{13}C NMR (75 MHz, $CDCl_3$) δ 31.38, 10.86, -10.09; ^{119}Sn NMR (112 MHz, $CDCl_3$) δ -0.30; MS (EI+, *M-15*) 367, 369, 371. The H[1] NMR and ^{119}Sn NMR spectra of the compound **(1b)** are consistent with the ones reported in the literature.[1,2]

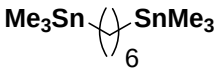

1,6-Bis(trimethylstannyl)hexane (2b). Following the above general procedure with 1,6 dibromohexane **2a** (1 ml, 6.50 mmol), Mg (1.6 g, 65.58 mmol) and trimethylstannyl chloride 1.0 M in THF (13.1 mL, 13.1 mmol), the crude reaction mixture was purified by column chromatography (hexane) to provide the colorless oil **2b** (900 mg, 2.18 mmol, 34%). ^{1}H NMR ($CDCl_3$, 300MHz, ppm) δ 1.62-142 (m, 4H), 1.35-1.22 (m, 4H), 0.95-0.65 (m, 4H), 0.05 (t, J = 24 Hz, 18H); ^{13}C NMR ($CDCl_3$, 75MHz, ppm) δ 33.81, 26.83, 11.31, -10.10; ^{119}Sn NMR (112 MHz, $CDCl_3$) δ -0.79; MS (EI+, *M-15*) 395, 397, 399. The H[1] NMR and ^{119}Sn NMR spectra of the compound **(2b)** are consistent with the ones reported in the literature.[1,2]

1,6-Bis(trimethylstannyl)octane (3b). Following the above general procedure with 1,8 dibromooctane **3a** (0.92 ml, 5.0 mmol), Mg (1.21 g, 50.0 mmol) and trimethylstannyl chloride 1.0 M in THF (10.0 ml, 10.0 mmol), the crude reaction mixture was purified by column chromatography (hexane) to provide the colorless oil **3b** (1.43 g, 3.25 mmol, 65%). ^{1}H NMR (300 MHz, $CDCl_3$) δ 1.74-1.36 (m, 4H), 1.27 (s, 8H), 0.97-0.66 (m, 4H), 0.26- -0.18 (m, 18H); ^{13}C NMR (75 MHz, $CDCl_3$) δ 34.20, 29.39, 26.83, 11.29, -10.15; ^{119}Sn NMR (112 MHz, $CDCl_3$) δ -0.40; MS (EI+, *M-15*) 427, 425, 423.

1,4-Bis(trimethylstannyl)nonane (4b). Following the above general procedure with 1,9 dibromononane **4a** (1 mL, 4.91 mmol), Mg (1.19 g, 49.1 mmol) and trimethylstannyl chloride 1.0 M in THF (9.82 mL, 9.82 mmol), the crude reaction mixture was purified by column chromatography (pentane) to provide the colorless oil **4b** (980 mg, 0.1875 mmol, 44%). ^{1}H NMR ($CDCl_3$, 400MHz, ppm) δ 1.60-1.40 (m, 4H), 1.35-1.25 (m, 10H), 0.95-0.70 (m, 4H), 0.04 (t, J = 24 Hz, 18H); ^{13}C NMR ($CDCl_3$, 75MHz, ppm) δ 34.15, 29.86, 29.43, 26.81, 11.24, -10.16; ^{119}Sn NMR (112 MHz, $CDCl_3$) δ 2.00; MS (EI+, *M-15*) 437, 439, 441.

1,10-Bis(trimethylstannyl)decane (5b). Following the above general procedure with 1,10 dibromodecane **5a** (1 mL, 4.44 mmol), Mg (1.06 g, 44.4 mmol) and trimethylstannyl chloride 1.0 M in THF (8.88 mL, 8.88 mmol), the crude reaction mixture was purified by column chromatography (pentane) to provide the colorless oil **5b** (1.2 g, 0.1875 mmol, 58%).

^{1}H NMR ($CDCl_3$, 300MHz, ppm) δ 1.60-1.45 (m, 4H), 1.35-1.20 (m, 12H), 0.95-0.70 (m, 4H), 0.04 (t, J = 27 Hz, 18H); ^{13}C NMR ($CDCl_3$, 75MHz, ppm) δ 34.23, 29.91, 29.47, 26.88, 11.13, -10.13; ^{119}Sn NMR (112 MHz, $CDCl_3$) δ -0.40; MS (EI+, *M-15*) 455, 453, 451.

1,12-Bis(trimethylstannyl)dodecane (6b). Following the above general procedure with 1,10 dibromodecane **6a** (1 g, 3.04 mmol), Mg (740 mg, 30.47 mmol) and trimethylstannyl chloride 1.0 M in THF (6.08 mL, 6.08 mmol), the crude reaction mixture was purified by column chromatography (pentane) to provide the colorless oil **6b** (1.1 g, 2.20 mmol, 72%). ^{1}H NMR ($CDCl_3$, 300MHz, ppm) δ 1.60-1.40 (m, 4H), 1.33-1.21 (m, 16H), 0.94-0.65 (m, 4H), 0.04 (t, J = 27 Hz, 18H); ^{13}C NMR ($CDCl_3$, 75MHz, ppm) δ 34.23, 29.90, 29.86, 29.49, 26.88, 11.31, -10.13; ^{119}Sn NMR (112 MHz, $CDCl_3$) δ -0.42; MS (EI+, *M-15*) 483, 481, 479.

1,4-Bis(trimethylstannyl)benzene (7):

Following the published procedure [3] with 1,4-diiobenzene (373 mg, 1.131 mmol), t-BuLi (1.7 M in pentane) (3.3 ml, 5.65 mmol) and trimethylstannylchloride (1.0 M in THF) (2.262 ml, 2.262 mmol) in THF (10 mL), the crude reaction mixture was purified by column chromatography (hexane) to provide the desired 1,4-bis(trimethylstannyl)benzene (320 mg, 0.79 mmol, 70%). ^{1}H NMR ($CDCl_3$, 300MHz, ppm) δ 7.50 (s, 4H), 0.56 - 0.00 (m, 18H); ^{13}C NMR (75 MHz, $CDCl_3$) δ 142.71, 136.03, -9.21; ^{119}Sn NMR (112 MHz, $CDCl_3$) δ -28.75. The NMR spectra of the compound (**7**) are consistent with the ones reported in the literature.[3]

1,4-Bis(triphenylphosphinylauryl)benzene (8):

Following the published procedure [4] with 1,4-diiobenzene (36 mg, 0.109 mmol), n-BuLi (1.6 M in hexane) (0.14 ml, 0.218 mmol) and chlorotriphenylphosphine gold(I)-complex (97 mg, 0.196 mmol) in ether (1 mL), the crude reaction mixture was re-crystallized in DCM/ EtOH to provide the desired 1,4-bis(triphenylphosphinylauryl) benzene with low yield. ^{1}H NMR (CD_2Cl_2, 300MHz, ppm) δ 7.65-7.36 (m, 34H); ^{31}P NMR (162 MHz, CD_2Cl_2) δ 39.87. The NMR spectra of the compound (**8**) are consistent with the ones reported in the literature.[4]

1,6-Bis(triphenylphosphinylauryl)hexane (9):

1,6-Bis(triphenylphosphinylauryl)hexane was prepared following a modified literature procedure[5] for 1,4-Bis(triphenylphosphinylauryl)butane. To a suspension of Mg(700mg, 29mmol) and a small crystal of I_2 in dry THF (10 mL) was added a solution of 1,6-dibromohexane (636mg, 2.6mmol) in THF (16 mL) over 3 h at room temperature. The resulting mixture was kept stirring for 3 h at this temperature. Then 1.5 mL of the above Grignard solution was added drop-wise to a solution of $(PPh_3)_3AuBr$ (108mg, 0.2mmol) in 5ml THF. The mixture was stirred overnight and the solvent was evaporated. Water (20ml) and dichloromethane (75ml) was added to the residue. Then the dichloromethane layer was washed 3 times with water (20ml). After drying with anhydrous sodium sulfate, the solvents were removed under vacuum. The crude oil was purified by reverse phase preparative HPLC (mobile phase: MeOH/H_2O/THF=75/10/15; flow rate 5 ml/min) to provide the off-white solid (**9**) (20mg, 0.02 mmol, 20%). m.p. 48 ^oC (decomp.); ^1H NMR (CD_2Cl_2, 400 MHz, ppm) δ 7.55-7.42 (m, 30H), 1.89-1.83 (m, 4H), 1.55-1.49 (m, 4H), 1.45-1.39 (m, 4H) ; ^{13}C NMR (100 MHz, CD_2Cl_2) δ 134.23 (d, J = 13.6 Hz), 131.90 (d, J = 44.6 Hz), 130.74 (d, J = 1.8 Hz), 128.87(d, J = 10.3 Hz), 36.93 (d, J = 4.6 Hz), 32.03 (d, J = 4.0 Hz), 31.29 (d, J = 94.6 Hz); ^{31}P NMR (162 MHz, CD_2Cl_2) δ 46.4 (s); HRMS (FAB) *m/z* calcd. for $C_{42}H_{42}Au_2P_2$ 1002.2093, found 1002.2097.

1,8-Bis(triphenylphosphinylauryl)octane (10):

Compound **10** was prepared following the procedure for 1,6-bis-(triphenylphosphinylauryl) hexane. The crude oil was purified by reverse phase preparative HPLC (mobile phase: MeOH/H_2O/THF=75/10/15; flow rate 5 ml/min) to provide the off-white solid (**10**) (24mg, 23%). m.p. 85 ^oC (decomp); ^1H NMR (CD_2Cl_2, 400MHz, ppm) δ 7.55-7.42 (m, 30H), 1.89-1.80 (m, 4H), 1.50-1.34 (m, 12H); ^{13}C NMR (100 MHz, CD_2Cl_2) δ 134.21 (d, J = 13.7 Hz), 131.87 (d, J = 44.9 Hz), 130.77 (d, J = 1.9 Hz), 128.87(d, J = 10.3 Hz), 36.91 (d, J = 4.6 Hz), 31.86 (d, J = 3.8 Hz), 31.09 (d, J = 94.8 Hz), 30.10 (s); ^{31}P NMR (162 MHz, CD_2Cl_2) δ 46.5 (s); HRMS (FAB) *(m+1)/z* calcd. for $C_{44}H_{47}Au_2P_2$ 1031.2484, found 1031.2473.

Measurement and Data Analysis:

The conductance of each molecule was measured using the STM-based break-junction technique, where an Au tip (Alfa Aesar, 99.999%) cut to be sharp is perpendicularly brought in and out of contact with a substrate of ~100 nm of gold (Alfa Aesar, 99.999%) evaporated onto cleaved mica disks. The substrate is mounted on a piezoelectric positioner (Mad City Labs), so that sub-angstrom resolution in position is achieved. During the entire break junction procedure, a small, constant bias (25-250 mV) is applied between the tip and the substrate while the current is measured (Keithley 428-Prog). Piezo control and data collection was performed using a National Instruments PXI Chassis System (with PXI-4461, PXI-6289) at 40 kHz and driven and managed with a custom-program using Igor Pro (Wavemetrics, Inc.).

The experimental set-up is kept under ambient conditions. For each experiment, the substrate is cleaned under UV/Ozone for 15 minutes prior to use. For every conductance trace measurement, the STM tip is first brought into hard contact with the substrate to achieve a conductance greater than ~ 10 G_0. At this point, the junction electrodes are pulled apart at a speed of 15 nm/s for 0.25 seconds. Conductance is measured as a function of tip-sample displacement to generate conductance traces. For each tip/substrate pair, at least one set of 1,000 traces of clean gold breaks is collected to ensure the system is clean. Then, the target molecule, dissolved in 1,2,4-trichlorobenzene (~10 mM) is deposited and over 10,000 conductance traces are collected for each of the molecules reported here. To determine the conductance of a molecule, every trace is binned linearly into conductance bins, without any data selection, and compiled into a single conductance histogram. The resultant peak in the histogram gives the most frequently measured value of molecular conductance. Every molecule was measured using multiple tip/substrate pairs, on different days to check for consistency and reproducibility.

Control Experiments: A series of control molecules were measured to reinforce the notions of $SnMe_3$ cleavage and the direct formation of direct Au-C bonds.

1. **1,9-bis(trimethylstannyl)nonane (C9):** To eliminate the possibility of odd/even effects, 1,9-bis(trimethylstannyl)nonane (**C9**) was synthesized and measured. The

conductance histogram and peak position for **C9** is shown in SI Figure S1, where we see no unusual odd/even effects.

2. **1,6-bis(triphenylstannyl)-hexane (C6SnPh$_3$)**: A tri-phenylated, rather than tri-methylated, version of **C6** was also synthesized (1,6-bis(triphenylstannyl)-hexane (**C6SnPh$_3$**)). The histogram for this molecule is also shown in SI Figure S1. We see no molecular peak, indicating that the steric bulk of the phenyl groups blocks the formation of molecular junctions, probably by inhibiting the accessibility of the Sn-C bond to the gold atoms on the electrode. As comparison, the conductance histogram for C6 is also included.

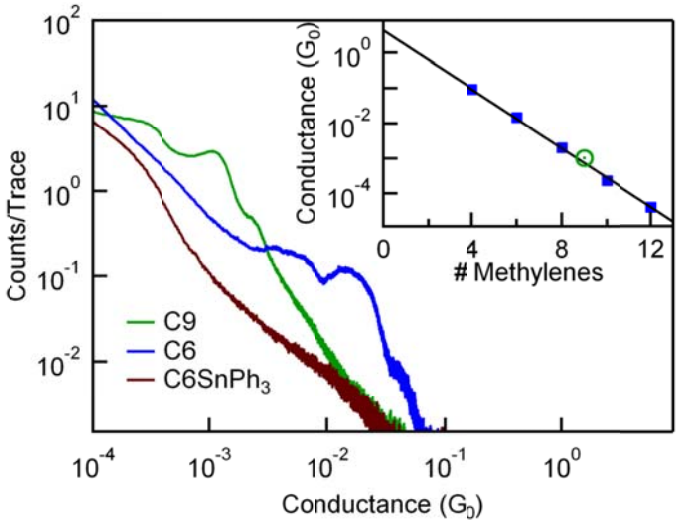

SI Figure S1: Conductance histograms for **C6SnPh$_3$**, **C6** and **C9**, generated from over 15000 conductance traces, without any data selection. Histogram bin size is $10^{-5}G_0$. Inset: Conductance histogram peak position versus number of methylene groups for all data in Figure 1D and for **C9** (green circle).

3. **Additional Experiments With 1,4-bis(trimethylstannyl) benzene (Ph):** Measurement of **Ph** did not show molecular plateaus during the first 2.5 hrs of measurements. In order to determine whether or not the reaction was triggered by the applied voltage, we introduced the ~1mM solution into the experimental set-up with the tip and substrate at equipotential (grounded) and waited for 3 hours before starting the measurements. We found conductance plateaus appeared immediately, indicating that a bias was not required during the wait period. This implies that the reaction is not voltage induced, but rather just stems from exposure of the target molecules to the gold surface. Second, we found that the length of the wait period depends weakly on

the concentration of the solution. When increasing the concentration of the solution by about 2 orders of magnitude, the waiting period decreased by only about half. This reaffirms that the mechanism behind the reaction is indeed surface chemistry, which means that exposure of the target molecule to the gold surface is essential to causing the transformation that facilitates measurement of conductance.

Data Analysis: In order to determine the percent of traces with steps, the following procedure was used. First, conductance cutoffs were designated using the conductance histograms for each molecule. The cutoffs were chosen to properly window the conductance peak (see example for **C6** in SI Figure S2).

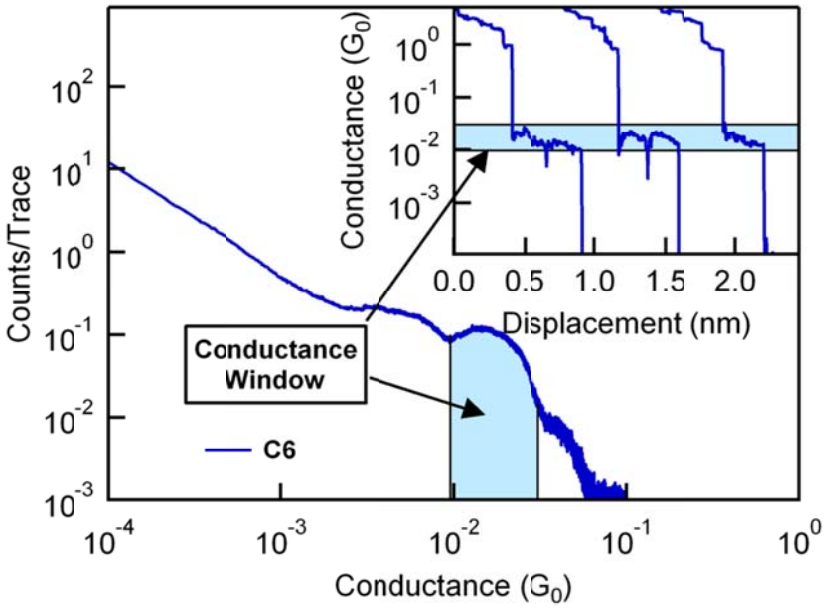

SI Figure S2: Conductance histogram for **C6** showing the peak region highlight the conductance window used to determine traces with conductance plateaus. Inset: Conductance window shown for sample traces.

The number of points in the conductance window was then counted for each trace, yielding a value for an equivalent molecular step length. If a particular trace has a step that is longer than 0.01 nm within the conductance window, we counted these traces as having a molecular plateau. For **C4,** 15% of all measured traces showed a conductance plateau. For **C6**, which is a slightly longer molecule, 30% of the traces showed a conductance plateau. The percentage of traces with **C8** plateaus when measuring the **C4** solution is about 50%, while a solution initially composed of **C8** yields 60%. The longer molecules, such as **C10** and **C12**, exhibit an almost 100% capture rate.

Many traces with molecular plateaus for **C6-C12** show dips to lower conductance value, as shown in manuscript Figure 1B. In contrast to molecular steps observed with amine-terminated or methylsulfide-terminated alkanes which are relatively flat and featureless, the molecular steps here show systematic dips at 2-2.5Å length intervals as the junction is elongated. To determine these length intervals, we select traces that have plateaus that are longer than 4Å. From the 16000 traces measured with **C6**, about 4800 had a molecular plateau, but only about 700 had a plateau longer than 4Å. After selecting this sub-set of 700 traces, we determined the length of each of the continuous segments within the entire molecular plateau (the distance between the dips) designated by the conductance window shown in SI Figure S2. In SI Figure S3, we plot a histogram of these continuous segment lengths. Two clear peaks are visible in this histogram indicating that continuous plateau lengths are around multiples of 2.1Å. As the length of the target molecule increases, the number of dips during each molecular step generally increases.

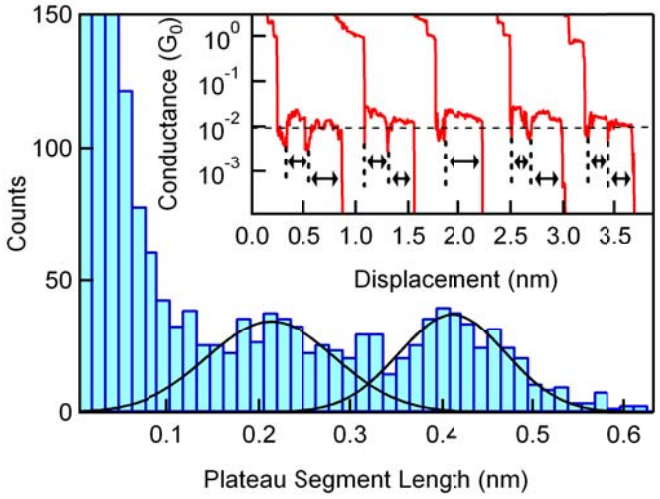

SI Figure S3: Histogram of the length of continuous plateau segments for **C6.** A total of 2682 plateau segments were determined from the selected 700 traces. Inset: Sample conductance traces showing individual segments.

Procedures for Theoretical Calculations

Bond Scission Energies:

The energy required to break CH_3-Sn and backbone-Sn bonds is calculated for isolated 1,4 bis(SnMe3)-terminated molecules using the Jaguar code with a lacv3p**++ basis set[6]. Spin-polarized total energy calculations are carried out using Density Functional Theory (DFT) with the generalized gradient approximation (PBE) implementation of exchange-correlation.[7]

The energy cost of cleaving a Me-Sn bond in $Sn(Me)_4$ is 3.09 eV. The results for breaking a Me-Sn or Sn-R bond in Me_3Sn-R-$SnMe_3$ molecules (with R=**C4**, **C6**, **C8** and **Ph**) are shown in SI Table S1. The energy needed to cleave a Me-Sn bond is independent of R. For alkanes, the Sn-R cleavage energy is approximately 0.3 eV smaller, independent of length. On the other hand, this result is reversed for **Ph**, where the Sn atom has an additional π coupling to the benzene states. Similar results are obtained with SIESTA, which was used for binding energy and transport calculations (see below for a description of the code).

R	C4	C6	C8	Ph
Me-Sn cleavage	3.07	3.08	3.07	3.04
Sn-R cleavage	2.79	2.80	2.79	3.25

SI Table S1: Energy (in eV) required to break a Me-Sn or the Sn-R molecular bond, as given by the total energy difference between the initial molecule and the sum of the cleaved products.

Binding Energy Calculations:

The binding of trimethyl tin alkanes to gold is calculated using SIESTA[8] with a double-zeta polarized basis set for the molecular atoms and a single-zeta polarized basis for Au (with high cutoff radii for tip and surface atoms). Total energy calculations are carried out using DFT with the GGA (PBE) implementation of exchange-correlation[7]. The electrode is modeled with a (111)-oriented slab that consists of five Au layers plus a few extra atoms to represent the tip. Periodic boundary conditions are imposed with a 5x5 unit cell (each Au layer containing 25 atoms) and slabs are separated by an appropriate vacuum region (~ 9 Å above the topmost atom in the adsorbate structure). The electronic structure is calculated at the Gamma point in the surface Brillouin zone using a 250 Ry

real-space cutoff in the calculation of the charge density and the solution of the Poisson equation. The geometry is relaxed until the forces on all molecule and tip atoms are less than 0.02 eV/Å.

Since bond scission energies are independent of alkane backbone length, we focus on the adsorption of a short alkane (Me_3Sn-C_2H_5). We compare two adsorption scenarios illustrated in Figure 3A and 3B respectively. In the first, the Sn-backbone bond scission followed by adsorption of the products. In the second, the Me-Sn bond scission is followed by adsorption of the products.

(A) $Au + Me_3Sn\text{-}R \rightarrow Au\text{-}R + Au\text{-}SnMe_3$

(B) $Au + Me_3Sn\text{-}R \rightarrow Au\text{-}SnMe_2\text{-}R + Au\text{-}Me$

We are primarily interested in the formation of junctions. We therefore consider binding of the backbone-containing fragment on the tip and several binding sites for the other fragment, for each scenario.

	Au surface Top	Au surface Bridge	Au surface Hollow	Au tip Top	Au tip Bridge
(A)	-0.82	-0.87	-0.86	-0.66	-0.71
(B)	-0.33	---	---	-0.63	---

SI Table S2: Binding energy (in eV) of product structures bound to Au following two scenarios: (A) backbone directly through an Au-C bond on the tip structure, with the $SnMe_3$ group on the Au surface or the tip (Figure 3A); (B) backbone through the Sn atom (Figure 3B) with the Me group on the Au surface on a top, bridge, or hollow site or on the tip structure.. Negative energies indicate that the final state is more energetically favorable. Note that the Me group does not bind on the bridge and hollow site on the Au surface, but moves to the top site as indicated in the table.

Energetics are detailed in SI Table S2 for both scenarios. In the first case (A), structures with the backbone bonded to the tip through Au – C bonds have a binding energy of ~0.8 eV regardless of whether the cleaved $SnMe_3$ group is adsorbed on a top, bridge or hollow site on the Au surface. Binding of the $SnMe_3$ group on a bridge or top position on the Au tip is slightly less favorable. In the second case (B), structures with the backbone bonded through Au – $SnMe_2$ – C bonds and a cleaved Me group show that the Me group will bind to just one Au atom (either an adatom or the atop site on the 111 surface). The binding energy is ~0.3 eV and ~0.6 eV when the Me group adsorbs on the surface and on

the Au tip, respectively. Starting geometries where the Me group was bound to hollow or bridge sites on the surface, or a bridge site on the tip, all relaxed to top configurations.

Transmission calculations:

Structural relaxation calculations of the molecular junctions are carried out using SIESTA[8] with initial structures containing the molecule and Au tips in a 4x4 Au(111) unit cell. The GGA (PBE) approximation is used for exchange-correlation[7]. Au atomic orbitals are described using single-zeta polarized orbitals (with high cutoff radii for tip and surface atoms) and molecular atoms are described by double-zeta polarized orbitals. Initially, the vertical distance is optimized by varying the electrode-electrode separation. The structure containing 6 Au layers is then optimized until the forces on all molecule and tip atoms are smaller than 0.02 eV/Å.

Subsequent transmission calculations are carried out using TranSIESTA [9] for relaxed geometries built from these optimized structures by adding 3 extra Au layers on each side of the supercell. The transport unit cell contains a total of Au 12 layers. The electronic structure is calculated using a 5x5 Monkhorst-Pack grid and a 250 Ry real-space cutoff. Transmission spectra are calculated with a 15x15 sampling of the transverse Brillouin zone. The effect of the electrode structure was investigated by checking these results against optimized structures bound to each Au electrode through a single adatom. The conductance at the Fermi level differed by ~7% and ~33% for **C6** and **Ph**, respectively, within the width of the experimental histograms.

Alkane junctions:

The conductance of alkanes when the molecular backbone R is bound directly to the Au tips is calculated for R=**C4**, **C6**, **C8** and for R=**C1,** for a frozen geometry. Their transmission spectra are shown in Figure 3D. The structure used for these calculations is shown in Figure 3C. The direct Au-C bond results in a broad 'end resonance' around -0.7 eV, which does not go to $1G_0$ but tails into the Fermi level yielding a relatively high conductance. This resonance corresponds to molecular states localized at the Au-molecule interface, as seen for alkanes with other linkers.[10,11] For longer alkanes, the height of this transmission peak decreases, as coupling across the junction decreases and

its width decreases slightly. Note that the position of this alkane peak with direct Au – C bonds is better coupled and closer to the Fermi level than with a variety of linkers, as reported from DFT-based calculations.[10,11]

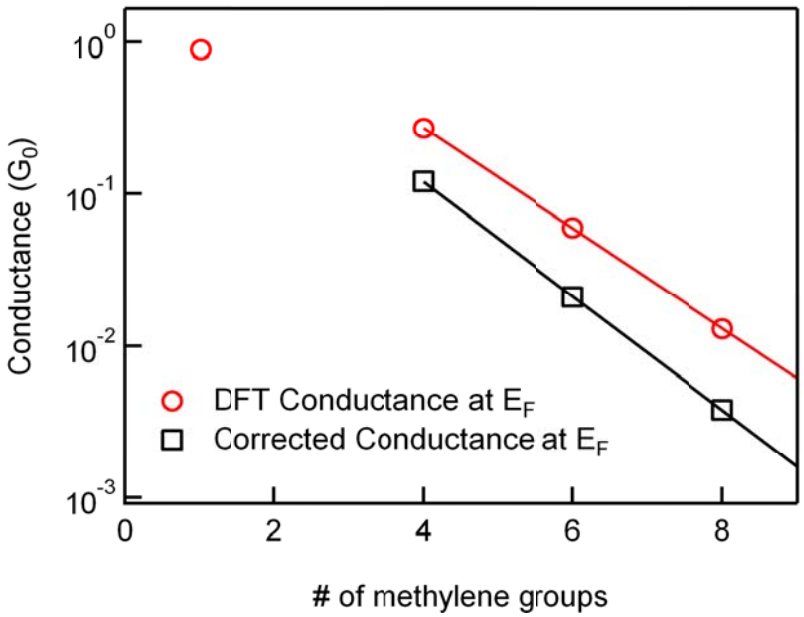

SI Figure S4: Calculated conductance versus number of methylene groups for **C1**, **C4**, **C6** and **C8** shown on a semi-log scale for DFT and corrected conductance values. Lines are exponential fits to the data.

The conductance at the Fermi level shows an exponential dependence with the number of methylene groups (see SI Figure S4). The calculated decay constant β, corresponding to $G \sim e^{-\beta N}$, is $\beta = 0.75$ per methylene group, indicating that transport is non-resonant. This is smaller than measured experimentally and slightly smaller than other calculated values.[10,11] Simple corrections to the position of the molecular resonance (detailed below) change this β to 0.87 per methylene, closer to the measured value.

Benzene junction:

The calculated transmission spectrum for **Ph** is compared to that for **C6** in SI Figure S5. The dashed lines further indicate the presence of two significant channels for the Ph case: σ and π. The two resonances occur at very similar energies (about –0.9 eV) with a total transmission larger than G_0. However, the π resonance is relatively narrow and the transmission at the Fermi energy is dominated by the σ channel (inset to SI Figure S5). These results agree with a recently published calculation based on similar methodology, when considering their 'adatom' case for benzene directly bonded to gold electrodes.[12]

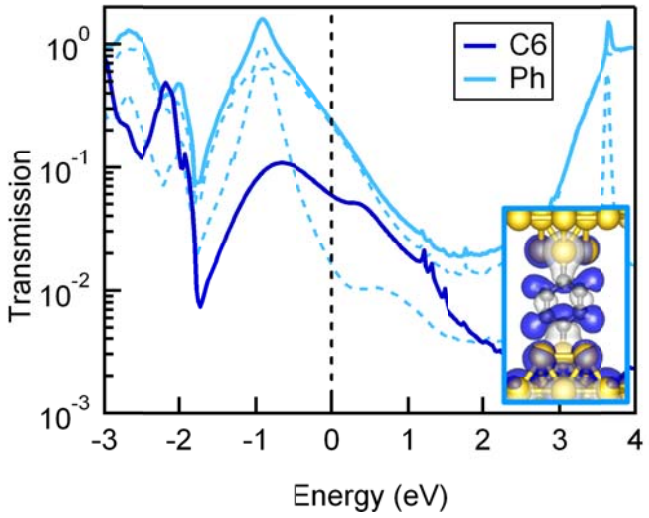

SI Figure S5: Calculated transmission spectra for **Ph** and **C6** shown on semi-log scale. Inset: transmission channel at the Fermi level calculated at the center of the Brillouin zone for **Ph**, showing the σ character of the resonance.

Corrections to molecular resonance position and conductance:

For non-resonant conductance, corrected conductance values can be estimated from DFT transmission results by shifting the dominant resonance rigidly to account for energy level misalignment in DFT associated with self-energy errors and image charge corrections.[13] The magnitude of the self-energy shift is calculated[6] by comparing the DFT orbital energy to the ionization potential calculated from the total energy difference of the neutral and charged molecule. For this system the molecule bound to two Au atoms (one on each end) is considered. The image charge correction is estimated by assuming the charge at the center of the molecule and taking the image plane 1Å above the Au(111) atomic plane.[14]

The net shift for the **Ph** σ resonance is -0.9 eV, which includes a downshift of -2.4 eV due to self-energy corrections and an upwards shift of 1.5 eV due to image charge corrections (See Table S3). Thus the relevant **Ph** resonance is downshifted from -0.9 eV to -1.8 eV; a single Lorentzian centered at this energy yields a conductance at the Fermi level of 0.054 G_0. This is to be compared to the DFT result of 0.24 G_0 and the measured value of 0.03 G_0.

For alkanes, the net downshift increases slightly with molecular length (-0.7 eV, -0.8 eV and -0.9 eV for **C4**, **C6** and **C8**, respectively) but, importantly, the resonances

initially around -0.7eV become narrower as the backbone length increases: their HWHM is 0.8 eV, 0.7 eV and 0.6 eV, respectively.

	C4	**C6**	**C8**	**Ph σ**	**Ph π**
Γ (eV)	0.82	0.71	0.61	0.50	0.14
Net level shift (eV)	-0.69	-0.82	-0.90	-0.90	-0.83

SI Table S3: Molecular resonance width determined from a Lorentzian fit and level shift including self-energy errors and image charge corrections.

The calculated DFT and corrected conductance values are compared to experiment in SI Table S4.

	C4	**C6**	**C8**	**Ph**
DFT	0.27	0.06	0.013	0.24
Corrected DFT	0.12	0.02	0.004	0.057
Experiment	0.093	0.014	0.002	0.03

SI Table S4: Calculated DFT and corrected conductance values, and experimentally measured results, for the molecules studied, in units of G_0.

References:

1. Bulten, E. J. & Budding, H. A. Synthesis of Small-Ring Monostannacycloalkanes. *J. Organomet. Chem.* **110**, 167-174 (1976).
2. Farah, D., Swami, K. & Kuivila, H. G. Synthesis and Spectral Characterization of Medium Ring Distannacycloalkanes and Their Lewis Acid-Derivatives. *J. Organomet. Chem.* **429**, 311-334 (1992).
3. Kaim, W., Tesmann, H. & Bock, H. Substituent Effects and Perturbation of Pi-Systems .36. Me3c-Substituted, Me3si-Substituted, Me3ge-Substituted, Me3sn-Substituted, and Me3pb-Substituted Benzene and Naphthalene Derivatives and Their Radical-Anions. *Chemische Berichte-Recueil* **113**, 3221-3234 (1980).
4. Flower, K. R., McGown, A. T., Miles, P. J., Pritchard, R. G. & Warren, J. E. Isolation of 1,4-Li-2-C6H4 and its reaction with [(Ph3P)AuCl]. *Dalton Transactions* **39**, 3509-3520 (2010).
5. Porter, K. A., Schier, A. & Schmidbaur, H. in Perspectives in Organometallic Chemistry (eds. Steele, B. R. & Screttas, C. G.) 74-85 (Royal Society of Chemistry 2003).
6. Jaguar v7.5 (Schrodinger, L.L.C., New York, NY 2008)

7. Perdew, J. P., Burke, K. & Ernzerhof, M. Generalized gradient approximation made simple. *Phys. Rev. Lett.* **77**, 3865-3868 (1996).
8. Soler, J. M. et al. The SIESTA method for ab initio order-N materials simulation. *J. Phys.:Cond. Mat.* **14**, 2745-2779 (2002).
9. Brandbyge, M., Mozos, J. L., Ordejon, P., Taylor, J. & Stokbro, K. Density-functional method for nonequilibrium electron transport. *Phys. Rev. B* **65**, 165401 (2002).
10. Li, C. et al. Charge transport in single Au vertical bar alkanedithiol vertical bar Au junctions: Coordination geometries and conformational degrees of freedom. *J. Am. Chem. Soc.* **130**, 318-326 (2008).
11. Sheng, W. et al. Quantum transport in alkane molecular wires: Effects of binding modes and anchoring groups. *J. Chem. Phys.* **131**, 244712 (2009).
12. Ma, G. H. et al. Low-bias conductance of single benzene molecules contacted by direct Au-C and Pt-C bonds. *Nanotechnology* **21**, 495202 (2010).
13. Quek, S. Y. et al. Amine-gold linked single-molecule circuits: Experiment and theory. *Nano Lett.* **7**, 3477-3482 (2007).
14. Smith, N. V., Chen, C. T. & Weinert, M. Distance of the Image Plane from Metal-Surfaces. *Phys. Rev. B* **40**, 7565-7573 (1989).